# State-Resolved Dynamics of the CN($B^2\Sigma^+$) and CH($A^2\Delta$) Excited Products Resulting from the VUV Photodissociation of $CH_3CN$†

**Chris R. Howle,‡ Alan N. Arrowsmith,‡,§ Viktor Chikan,# and Stephen R. Leone*,‡**

*Departments of Chemistry and Physics, University of California and Lawrence Berkeley National Laboratory, Berkeley, California 94720, Department of Chemistry and Biochemistry, University of Colorado, Boulder, Colorado 80309, and Department of Chemistry, Kansas State University, 111 Willard Hall, Manhattan, Kansas 66506*

*Received: December 12, 2006; In Final Form: January 18, 2007*

Fourier transform visible spectroscopy, in conjunction with VUV photons produced by a synchrotron, is employed to investigate the photodissociation of $CH_3CN$. Emission is observed from both the CN($B^2\Sigma^+-X^2\Sigma^+$) and CH($A^2\Delta-X^2\Pi$) transitions; only the former is observed in spectra recorded at 10.2 and 11.5 eV, whereas both are detected in the 16 eV spectrum. The rotational and vibrational temperatures of both the CN($B^2\Sigma^+$) and CH($A^2\Delta$) radical products are derived using a combination of spectral simulations and Boltzmann plots. The CN($B^2\Sigma^+$) fragment displays a bimodal rotational distribution in all cases. $T_{rot}$(CN($B^2\Sigma^+$)) ranges from 375 to 600 K at lower $K'$ and from 1840 to 7700 K at higher $K'$ depending on the photon energy used. Surprisal analyses indicate clear bimodal rotational distributions, suggesting CN($B^2\Sigma^+$) is formed via either linear or bent transition states, respectively, depending on the extent of rotational excitation in this fragment. CH($A^2\Delta$) has a single rotational distribution when produced at 16 eV, which results in $T_{rot}$(CH($A^2\Delta$)) = 4895 ± 140 K in $v' = 0$ and 2590 ± 110 K in $v' = 1$. From thermodynamic calculations, it is evident that CH($A^2\Delta$) is produced along with CN($X^2\Sigma^+$) + $H_2$. These products can be formed by a two step mechanism (via excited $CH_3$* and ground state CN($X^2\Sigma^+$)) or a process similar to the "roaming" atom mechanism; the data obtained here are insufficient to definitively conclude whether either pathway occurs. A comparison of the CH($A^2\Delta$) and CN($B^2\Sigma^+$) rotational distributions produced by 16 eV photons allows the ratio between the two excited fragments at this energy to be determined. An expression that considers the rovibrational populations of both band systems results in a CH($A^2\Delta$):CN($B^2\Sigma^+$) ratio of (1.2 ± 0.1):1 at 16 eV, thereby indicating that production of CH($A^2\Delta$) is significant at 16 eV.

## 1. Introduction

In this paper, the photofragmentation dynamics of $CH_3CN$ in highly energetic states (10−16 eV) are investigated. The results of this study are pertinent to several complex chemical systems. For example, nitrile species, such as $CH_3CN$ (acetonitrile), are involved in chemical mechanisms of relevance to combustion processes as reaction byproducts and flame additives.[1,2] Indeed, $CH_3CN$ has recently been detected as a constituent of vehicle exhaust fumes.[3] These environments are generally characterized by elevated temperatures (ca. $10^3$ K), thereby enabling the formation of highly energized species that can act as reactive intermediates. A typical example found in combustion reactions is the excited CH($A^2\Delta$) radical, which is produced from a variety of different reactions of hydrocarbon precursors.[4−7] The transition between this electronically excited-state and the corresponding ground state, CH($X^2\Pi$), is believed to be responsible for the blue emission observed in hydrocarbon flames. The CH radical can be studied in situ using optical methods; for instance, laser-induced fluorescence (LIF)[8,9] or degenerate four-wave mixing[9] for CH($X^2\Pi$), cavity ring down[10] or emission spectroscopy[11] for CH($A^2\Delta$). The resultant data from these experiments yield information on the CH radical concentrations and the extent of rotational and vibrational excitation in this species, thereby providing mechanistic details. In conjunction with laboratory kinetic measurements and comprehensive theoretical investigations, these data drive the knowledge of combustion chemistry toward greater levels of refinement.

$CH_3CN$ is also detected in the interstellar medium and in the atmosphere of Titan, Saturn's largest moon.[12,13] The photolysis of $CH_3CN$ by solar UV radiation can occur in these exotic environments,[14−16] as well as in diffuse interstellar clouds.[17] At photon energies near the dominant Lyman-α line at 10.2 eV these processes liberate the CN radical, an intermediate in the chemical scheme of Titan.[18] Experiment and theory show that this scheme results in the production of higher molecular weight nitriles and, after polymerization processes, the aerosol particles that form a stratospheric haze layer around this celestial body.[19−21] Recent studies suggest that further investigation into the product identities and abundances resulting from processes involving nitrile species is necessary to improve the accuracy of models detailing Titan's atmospheric chemistry.[18,22] Furthermore, CN provides a mechanism for incorporating nitrogen into the ring structure of polycyclic aromatic hydrocarbons to form polycyclic aromatic nitrogen heterocycles (PANHs).[23] Much improved fits to a 6.2 μm interstellar emission feature can be achieved by considering PANHs;[24] thus these species may provide a route to understanding the origins of the diffuse interstellar bands.[25] The need for additional spectroscopic studies

† Part of the special issue "M. C. Lin Festschrift".
‡ University of California and Lawrence Berkeley National Laboratory.
§ University of Colorado.
# Kansas State University.

10.1021/jp068544w CCC: $37.00 
Published on Web 03/20/2007

of excited species relevant to astrochemistry has also recently been noted.[26] Therefore, knowledge of how $CH_3CN$ interacts with VUV radiation, where the formation of electronically excited products is possible, will provide insight into the fragmentation mechanisms that occur in these chemical systems. Monitoring the resultant emission from the excited CH* and CN* radicals produced by photodissociation of $CH_3CN$ could provide a link between the hydrocarbon and nitrile chemical cycles that are prevalent in Titan's atmosphere.[18]

Furthermore, the dynamics of producing such radicals can also be studied on a fundamental level using photodissociation methods. In highly energized states, new mechanisms can occur. For example, recent theoretical and experimental studies of the UV photodissociation of $H_2CO$ have reported two distinct fragmentation mechanisms.[27,28] The first is the conventional pathway over the transition state barrier, to form vibrationally cold $H_2$ and rotationally hot CO; the second is a new route that circumvents this barrier, producing vibrationally hot $H_2$ and rotationally cold CO. The latter of these mechanisms starts with simple C−H bond fission, with the resultant H atom exploring the potential surface at distances up to several angstroms from the HCO fragment. This loosely bound hydrogen turns back toward HCO and abstracts the other H atom. The scheme detailed above is deemed the "roaming" atom mechanism;[27,28] note that more conventional dissociation pathways leading to H + HCO and H + H + CO are also possible as a result of UV photolysis. Similarly, in the reaction of $CH_3$ + O, an unexpected pathway leading to CO + $H_2$ + H via HCO + $H_2$ is observed, thus departing from the typical minimum energy path that leads to $H_2CO$ + H.[29] These unorthodox processes have also been shown to occur in $CH_3CHO$, where the methyl group is the "roaming" moiety.[30] Such extreme departures from classical transition state theory could herald a new class of molecular dynamics resulting in further opportunities for investigation. Numerous high photon energy dissociation processes in polyatomic molecules like $CH_3CN$ can lead to multiple bond breaking pathways that embody similar effects.

Previous fundamental research on the $CH_3CN$ molecule in the VUV region includes several photoabsorption studies using noble gas resonance lamps[31] and synchrotron light sources.[14,32,33] Mitsuke and Mizutani utilized a novel synchrotron pump−LIF probe scheme to study the ground state CN($X^2\Sigma^+$) radicals produced when $CH_3CN$ interacts with 13.6−18.6 eV photons.[34] Cody et al. used an argon lamp pump−LIF probe experiment to examine the CN($X^2\Sigma^+$) fragments produced at $h\nu$ < 9.5 eV under high collision frequency conditions ($P$ = 133 Pa).[35] Ashfold and Simons[36] and Moriyama et al.[37] have performed some work that is most pertinent to this study; comparisons to the findings of these two studies will be performed in this article. In the former case, $CH_3CN$ was excited with 8.79, 9.50, and 10.03 eV photons and the resultant CN($B^2\Sigma^+-X^2\Sigma^+$) fluorescence displayed a bimodal rotational distribution at all photon energies. This result can be attributed to dissociation from a linear transition state to form the low rotational levels and via a bent transition state to produce the higher rotational levels.[36] Emission from CN($B^2\Sigma^+-X^2\Sigma^+$) was measured after excitation by 10.2 eV photons in the latter study. Only a single rotational distribution can be ascertained from the rotational populations,[37] in contrast to the results of Ashfold and Simons. This disparity may be credited to the relatively modest resolution used in the work of Moriyama et al. of ≈13 $cm^{-1}$, which is approximately one order of magnitude larger than that employed in the other study. Other related investigations include reactions of $CH_3CN$ with metastable Ar($^3P_2$) atoms or $Ar^+$ ions in a flowing afterglow, where CH($A^2\Delta-X^2\Pi$) emission is observed.[38,39] Rotational temperatures for both reactions were subsequently derived.

In response to the various chemical issues raised above, we present the photofragment emission spectroscopy and dynamics resulting from the interaction of 10.2, 11.5, and 16 eV photons with gaseous $CH_3CN$. The signals resulting from both CN($B^2\Sigma^+-X^2\Sigma^+$) and CH($A^2\Delta-X^2\Pi$) transitions centered at 25,798 and 23,218 $cm^{-1}$, respectively, are collected by a Fourier transform visible (FTVIS) spectrometer. The multiplex advantage intrinsic to interferometers permits both of these emission signals to be simultaneously monitored.[40] In addition, the available resolution allows the rotational and vibrational populations and temperatures to be derived. It is observed that the rotational distribution in CN($B^2\Sigma^+$) is bimodal in all of the acquired spectra, therefore supporting the mechanism detailed by Ashfold and Simons.[37] However, the signal from the CH($A^2\Delta$) radical only displays a single rotational distribution. Thermochemical calculations indicate that the CH($A^2\Delta$) excited fragment is formed in combination with ground state CN($X^2\Sigma^+$) and molecular hydrogen. The ratio between CH($A^2\Delta$) and CN($B^2\Sigma^+$) is obtained for photolysis at 16 eV, where both emission signals are observed, and equals (1.2 ± 0.1):1.

## 2. Experimental Method

The FTVIS apparatus employed in this study has been described in detail elsewhere,[41] so only the salient features will be mentioned here. The experiments are conducted at beamline 9.0.2 of the Advanced Light Source, Berkeley, CA, which can provide 8−30 eV photons when operating at a beam energy of 1.9 GeV.[42] $CH_3CN$ pressures of ≈9 Pa are used in a sample chamber and two stages of differential pumping maintain a base pressure of ca. 6 × $10^{-7}$ Pa in the beamline monochromator. The horizontally polarized VUV photons from the beamline pass through these vacuum stages and into a continuously evacuated sample chamber, where interactions with gaseous $CH_3CN$ result in the emission from excited states of diatomic fragments. This light exits the evacuated environment perpendicular to the incident light via a collimating lens and a window in the base of the chamber. Initially, the action spectrum of $CH_3CN$ is recorded as a function of photon energy in the 8−24 eV region using a broadband photomultiplier tube (PMT, Hamamatsu R955, $\lambda$ = 160−900 nm or 11,111−62,500 $cm^{-1}$) placed directly underneath the output window. To collect the rotationally resolved spectra, the emission is steered to the horizontal plane by a 45° protected aluminum mirror (CVI Laser Corp. part no. PAUV-PM-2037-C) located below the output window, followed by a further three protected aluminum mirrors for fine alignment, and focused into the entrance port of the FTVIS spectrometer. All of the aforementioned optics are contained in a light-tight box and a contracted iris is used to reduce the field of view into the spectrometer; the latter procedure improves the resolution of the acquired spectra, because the resolving power $R = 2\pi/\Omega$, where $\Omega$ is the solid angle.[40,43] The FTVIS device is an adapted Bruker IFS 66v/s spectrometer equipped with a $CaF_2$ beamsplitter (Bruker T 602/8A, output light is ca. 60% horizontally polarized) and a UV/vis PMT (Electron Tubes 9813B). Spectra can be collected in the 300−600 nm (16,667−33,333 $cm^{-1}$) wavelength range at a fixed VUV photon energy using this configuration. An instrument response function of the collection apparatus is obtained by acquiring a spectrum of a quartz tungsten halogen lamp and comparing it to a standard reference spectrum of the same lamp; all of the data are corrected using this response curve. The movable mirror within

**TABLE 1: Thermochemical Thresholds for Channels Resulting in Either UV/Visible Emission Detectable by the FTVIS Spectrometer or Nonradiative Dissociation after VUV Excitation of $CH_3CN$[a]**

| products | $\Delta H^0_{298}$ (eV) | possible emission channel(s) |
|---|---|---|
| $CH_2CN + H$ | 4.03 | |
| $HCCN + H_2$ | 4.25 | |
| $CH_3 + CN(X^2\Sigma^+)$ | 5.26 | |
| $HCCN + 2H$ | 6.51 | |
| $C_2H_3 + N$ | 7.24 | |
| $C_2N + H_2 + H$ | 7.27 | |
| $CH_3 + CN(B^2\Sigma^+)$ | 8.45 | $CN(B^2\Sigma^+-X^2\Sigma^+)$ |
| $CH(X^2\Pi) + CN(X^2\Sigma^+) + H_2$ | 9.91 | |
| $CH_2 + CN(X^2\Sigma^+) + H$ | 10.02 | |
| $C_2N + 3H$ | 11.79 | |
| $CH(A^2\Delta) + CN(X^2\Sigma^+) + H_2$ | 12.78 | $CH(A^2\Delta-X^2\Pi)$ |
| $CH(X^2\Pi) + CN(B^2\Sigma^+) + H_2$ | 13.10 | $CN(B^2\Sigma^+-X^2\Sigma^+)$ |
| $CH(B^2\Sigma^-) + CN(X^2\Sigma^+) + H_2$ | 13.14 | $CH(B^2\Sigma^--X^2\Pi)$ |
| $CH_2 + CN(B^2\Sigma^+) + H$ | 13.21 | $CN(B^2\Sigma^+-X^2\Sigma^+)$ |
| $CH(C^2\Sigma^+) + CN(X^2\Sigma^+) + H_2$ | 13.85 | $CH(C^2\Sigma^+-X^2\Pi)$ |
| $CH(X^2\Pi) + CN(X^2\Sigma^+) + 2H$ | 14.43 | |
| $C_2(X^1\Sigma_g^+) + N + H_2 + H$ | 15.09 | |
| $CH(A^2\Delta) + CN(B^2\Sigma^+) + H_2$ | 15.98 | $CH(A^2\Delta-X^2\Pi)$, $CN(B^2\Sigma^+-X^2\Sigma^+)$ |
| $CH(B^2\Sigma^-) + CN(B^2\Sigma^+) + H_2$ | 16.33 | $CH(B^2\Sigma^--X^2\Pi)$, $CN(B^2\Sigma^+-X^2\Sigma^+)$ |
| $CH(C^2\Sigma^+) + CN(B^2\Sigma^+) + H_2$ | 17.04 | $CH(C^2\Sigma^+-X^2\Pi)$, $CN(B^2\Sigma^+-X^2\Sigma^+)$ |
| $CH(A^2\Delta) + CN(X^2\Sigma^+) + 2H$ | 17.31 | $CH(A^2\Delta-X^2\Pi)$ |
| $CH(X^2\Pi) + CN(B^2\Sigma^+) + 2H$ | 17.62 | $CN(B^2\Sigma^+-X^2\Sigma^+)$ |
| $CH(B^2\Sigma^-) + CN(X^2\Sigma^+) + 2H$ | 17.66 | $CH(B^2\Sigma^--X^2\Pi)$ |
| $CH(C^2\Sigma^+) + CN(X^2\Sigma^+) + 2H$ | 18.37 | $CH(C^2\Sigma^+ - X^2\Pi)$ |
| $C_2(X^1\Sigma_g^+) + N + 3H$ | 19.61 | |
| $CH(A^2\Delta) + CN(B^2\Sigma^+) + 2H$ | 20.50 | $CH(A^2\Delta-X^2\Pi)$, $CN(B^2\Sigma^+-X^2\Sigma^+)$ |
| $CH(B^2\Sigma^-) + CN(B^2\Sigma^+) + 2H$ | 20.85 | $CH(B^2\Sigma^--X^2\Pi)$, $CN(B^2\Sigma^+-X^2\Sigma^+)$ |
| $CH(C^2\Sigma^+) + CN(B^2\Sigma^+) + 2H$ | 21.57 | $CH(C^2\Sigma^+ - X^2\Pi)$, $CN(B^2\Sigma^+-X^2\Sigma^+)$ |

[a] Values of enthalpies of formation and excited-state energies are taken from standard literature sources,[45,66] apart from the $\Delta_f H^0_{298}$ value for HCCN.[71]

the interferometer is operated in continuous scan mode at a frequency of 20 kHz, thus negating the effect of the gradually reduced synchrotron beam current during the duration of the scan (generally 2−4 h). Higher order VUV radiation is eliminated from the synchrotron beam by the use of a gas filter containing either argon or helium that is installed on the beamline.[44] Using these noble gases, experiments with purely first-order light are possible up to 15.8 and 24.6 eV, respectively. A photon energy resolution of 0.1 eV is employed throughout this study. The photon energy calibration of the beamline monochromator is verified by measuring the appearance of emission from nitrogen at 25,566 $cm^{-1}$ due to the $N_2^+$ ($B^2\Sigma_u^+-X^2\Sigma_g^+$) transition, whose onset is quoted as 18.75 eV in the literature,[45,46] using the broadband PMT. Reagent grade (purity ≥99.5%) $CH_3CN$, obtained from Sigma-Aldrich, is introduced into a high vacuum compatible glass bottle in a dry nitrogen atmosphere. The sample is subjected to several freeze−pump−thaw cycles prior to use.

## 3. Results

**3.1. UV/Vis Action Spectrum of $CH_3CN$.** The accessible emissive channels can be predicted using simple thermochemical calculations. These values, in combination with the total emission (or action) spectrum as a function of $h\nu$, display which emitting pathways are dominant in a given photon energy region. The following section uses these data to elucidate what experiments are possible with the FTVIS apparatus. Table 1 contains the photodissociation channels that result in either emission detectable with the FTVIS apparatus or bond cleavage to form ground state products. Table 2 lists the higher electronically excited states of the CH*, CN*, and $C_2$* fragments that can be produced in the VUV photon energy range studied here. At low photon energies, single or multiple bond fission is possible, with loss of one or more hydrogen atom(s) favored. From a comparison of the $\Delta H^0_{298}$ values for the $CH_3 + CN(X^2\Sigma^+)$ and $C_2H_3 + N$ channels, it is clear that cleavage of the C−C single bond requires 2 eV less energy than C≡N triple bond fission. Further fragmentation can take place using higher photon energies, where channels forming electronically excited diatomics are also accessible. Emission from electronically excited $C_2$* is only energetically feasible above 17.57 eV; therefore, emission from excited CH* and CN* fragments dominates when excitation occurs with $h\nu < 17.57$ eV. Indeed, no $C_2^*$ emission bands are observed in any of the spectra recorded at $h\nu = 10.2$, 11.5, and 16 eV using the FTVIS spectrometer. The VUV action spectrum for $CH_3CN$ where $h\nu = 8-24$ eV is shown in Figure 1. As seen in Table 2, formation of CH* and CN* in excited electronic states up to the $E^2\Pi$ state and the $F^2\Delta$ state, respectively, is possible with 8−24 eV photons and emission from these states could be detected by the broadband PMT. Note that the CN($A^2\Pi-X^2\Sigma^+$) transition is not considered in this work, because its band center occurs at 1097 nm (9117 $cm^{-1}$), which is outside of the detection window of the apparatus. The onset of emission signal is observed in the action spectrum at a photon energy of 8.9 ± 0.1 eV with substantial signal observed in the ca. 9.5−13.5 eV region. The peak of maximum intensity occurs at 11.8 ± 0.1 eV, which is surrounded by peaks at 10.0, 10.2, 10.5, 10.9, 11.5, and 12.4 eV. The CN($B^2\Sigma^+-X^2\Sigma^+$) fluorescence cross section has been observed to mimic the total photoabsorption cross section up to ≈13 eV in several previous studies of $CH_3CN$.[14,31,33] According to Table 1, we can assume that the CN($B^2\Sigma^+-X^2\Sigma^+$) transition is the dominant source of emission contributing to the action spectrum up to ≈ 13 eV. Therefore, in accordance with the previous absorption data,[14,31−33] it is reasonable to assign the observed discrete features as Rydberg transitions that converge to the first ionization potential of the parent molecule at 12.20 eV.[45] Precise labeling of this structure

**TABLE 2: Thermochemical Thresholds for Channels Resulting in Higher Electronically Excited States of the CH*, CN*, and $C_2$* Radicals after VUV Excitation of $CH_3CN$[a]**

| products | $\Delta H^0_{298}$ (eV) |
|---|---|
| $CH_3 + CN(D^2\Pi)$ | 12.01 |
| $CH_3 + CN(E^2\Sigma^+)$ | 12.59 |
| $CH_3 + CN(F^2\Delta)$ | 12.71 |
| $CH_3 + CN(G^2\Pi)$ | 12.90 |
| $CH_3 + CN(H^2\Pi)$ | 12.94 |
| $CH_3 + CN(J^2\Delta)$ | 13.35 |
| $CH(X^2\Pi) + CN(D^2\Pi) + H_2$ | 16.66 |
| $CH(X^2\Pi) + CN(E^2\Sigma^+) + H_2$ | 17.24 |
| $CH(X^2\Pi) + CN(F^2\Delta) + H_2$ | 17.36 |
| $CH(X^2\Pi) + CN(G^2\Pi) + H_2$ | 17.55 |
| $CH(X^2\Pi) + CN(H^2\Pi) + H_2$ | 17.59 |
| $CH(X^2\Pi) + CN(J^2\Delta) + H_2$ | 18.00 |
| $CH_2 + CN(D^2\Pi) + H$ | 16.77 |
| $CH_2 + CN(J^2\Delta) + H$ | 18.11 |
| $CH(D^2\Pi) + CN(X^2\Sigma^+) + H_2$ | 17.40 |
| $CH(D^2\Pi) + CN(B^2\Sigma^+) + H_2$ | 20.59 |
| $CH(D^2\Pi) + CN(X^2\Sigma^+) + 2H$ | 21.92 |
| $CH(D^2\Pi) + CN(B^2\Sigma^+) + 2H$ | 25.11 |
| $CH(E^2\Pi) + CN(X^2\Sigma^+) + H_2$ | 18.05 |
| $CH(E^2\Pi) + CN(B^2\Sigma^+) + H_2$ | 21.24 |
| $CH(E^2\Pi) + CN(X^2\Sigma^+) + 2H$ | 22.57 |
| $CH(E^2\Pi) + CN(B^2\Sigma^+) + 2H$ | 25.76 |
| $CH(F^2\Sigma^+) + CN(X^2\Sigma^+) + H_2$ | 18.09 |
| $CH(F^2\Sigma^+) + CN(B^2\Sigma^+) + H_2$ | 21.28 |
| $CH(F^2\Sigma^+) + CN(X^2\Sigma^+) + 2H$ | 22.61 |
| $CH(F^2\Sigma^+) + CN(B^2\Sigma^+) + 2H$ | 25.80 |
| $C_2(d^3\Pi_g) + N + H_2 + H$ | 17.57 |
| $C_2(C^1\Pi_g) + N + H_2 + H$ | 19.33 |
| $C_2(e^3\Pi_g) + N + H_2 + H$ | 20.15 |
| $C_2(D^1\Sigma_u^+) + N + H_2 + H$ | 20.45 |
| $C_2(E^1\Sigma_g^+) + N + H_2 + H$ | 21.91 |
| $C_2(d^3\Pi_g) + N + 3H$ | 22.09 |
| $C_2(C^1\Pi_g) + N + 3H$ | 23.86 |
| $C_2(e^3\Pi_g) + N + 3H$ | 24.67 |
| $C_2(D^1\Sigma_u^+) + N + 3H$ | 24.97 |
| $C_2(E^1\Sigma_g^+) + N + 3H$ | 26.43 |

[a] Values of enthalpies of formation and excited-state energies are taken from standard literature sources.[45,66]

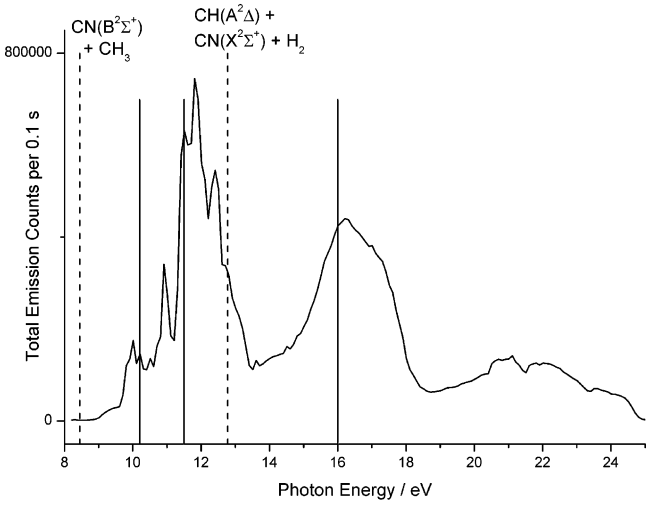


**Figure 1.** Action spectrum of $CH_3CN$ in the 8−24 eV region acquired with a photon energy resolution of 0.1 eV. The lowest energy thresholds for forming the $CN(B^2\Sigma^+)$ and $CH(A^2\Delta)$ excited products are indicated by dashed lines, and the photon energies used in the experiment are denoted by gray lines.

is not possible at the resolution used to acquire the data presented in Figure 1. Autoionization is possible from high lying Rydberg levels, although there have been no reports of bands in the photoelectron spectrum at energies less than 12.20 eV.[47−49]

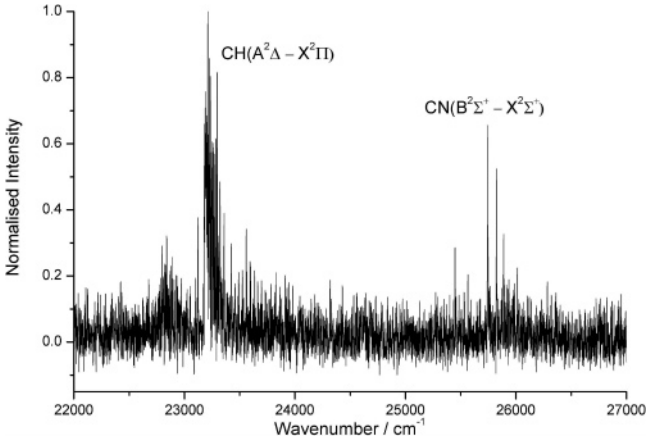


**Figure 2.** FTVIS spectrum acquired at $h\nu = 16$ eV showing emission due to the $CH(A^2\Delta-X^2\Pi)$ and $CN(B^2\Sigma^+-X^2\Sigma^+)$ transitions.

A further intense, broad peak is detected between 14.5−18 eV, with a maximum at 16.2 ± 0.1 eV. The lack of defined structure is in harmony with the absorption spectrum of $CH_3CN$, which is a continuum at $h\nu > 13$ eV.[31,33] This feature displays a profile over the same photon energy range nearly identical to that seen in the $CN(B^2\Sigma^+ - X^2\Sigma^+)$ excitation spectrum recorded by Mitsuke and Mizutani.[34] Because their detection PMT is rated to cover the 300−650 nm (15,584−33,333 $cm^{-1}$) range, which is narrower than that of the broadband PMT used here, transitions that emit at longer or shorter emission wavelengths are unlikely to be observed in the 14.5−18 eV photon energy region displayed in Figure 1. Therefore, when the relevant thermochemistry is also considered (Tables 1 and 2), it is highly probable that the broad feature comprises emission from the $CN(B^2\Sigma^+)$, $CH(A^2\Delta)$, $CH(B^2\Sigma^-)$, and $CH(C^2\Sigma^+)$ excited states to their respective ground states. The band centers of these transitions occur at 25,798, 23,218, 26,598, and 31,778 $cm^{-1}$, respectively.[45] A smaller broad feature is observed above 20 eV excitation energy, which is likely to consist of an amalgamation of emission signals from excited states of the $C_2$*, CN*, and CH* fragments. This higher photon energy range is not the primary focus of this study, so it will not be discussed further.

**3.2. Rotationally Resolved Spectra of $CN(B^2\Sigma^+-X^2\Sigma^+)$ and $CH(A^2\Delta-X^2\Pi)$.** The rotational and vibrational populations in the electronically excited states of CN* and CH* can be obtained by comparing emission spectra acquired with the FTVIS spectrometer to spectral simulations. By using these derived populations in Boltzmann plots, we can obtain the rotational and vibrational temperatures. Surprisal analyses indicate how the extent of excitation in the observed fragment compares to a statistical prediction, thereby providing insight into the dissociation dynamics at a given photon energy. Spectra are acquired using the FTVIS spectrometer and incident photon energies of 10.2, 11.5, and 16 eV; the spectrum acquired at a photon energy of 16 eV is shown in Figure 2. These energies correspond to the Lyman−α hydrogen line (the principal UV line observed from solar radiation), and the peaks of the two main emission features observed in the action spectrum (Figure 1), respectively. Emission from the $CN(B^2\Sigma^+-X^2\Sigma^+)$ transition is observed in all of these spectra, as shown in Figures 3a, 4a, and 5a. The characteristic P band heads for the $\Delta v = 0$ series of transitions are clearly apparent in all of the spectra; up to the (3,3) vibrational band in the 11.5 and 16 eV spectra, as labeled. The corresponding R branches are of lower intensity and are obscured by the band head of the P branch for the adjacent band, e.g., the R(0,0) lines merge with the P(1,1) band

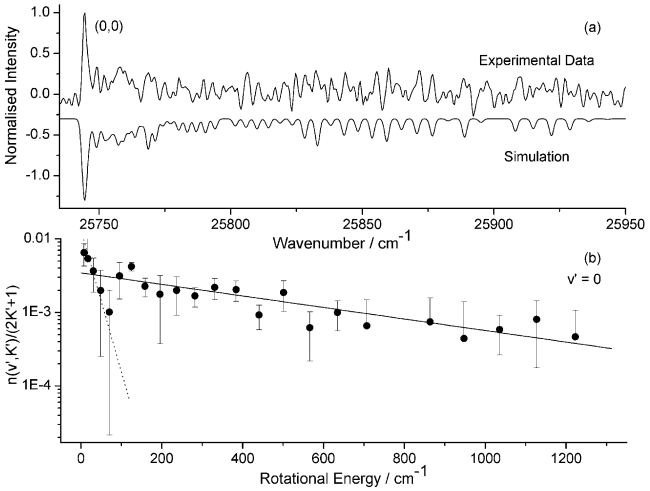


**Figure 3.** (a) Experimental and simulated spectra of the CN($B^2\Sigma^+-X^2\Sigma^+$) transition resulting from photodissociation of $CH_3CN$ at 10.2 eV. The simulated spectrum is inverted for clarity. (b) Boltzmann plot of the rotational populations in the $v' = 0$ level versus the available rotational energy. The dotted line denotes a fit originating from weak rotational bands.

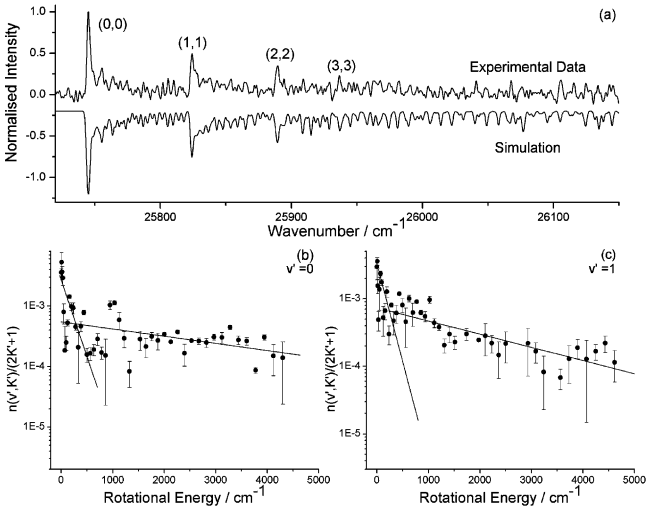


**Figure 4.** (a) Experimental and simulated spectra of the CN($B^2\Sigma^+-X^2\Sigma^+$) transition resulting from photodissociation of $CH_3CN$ at 11.5 eV. The simulated spectrum is inverted for clarity. (b), (c) Boltzmann plots of the rotational populations in the $v' = 0$ or 1 level versus the available rotational energy.

head. This effect, magnified by the limited signal-to-noise ratios near some of the band origins, means that the profiles of the P branches are central to the assignment of rotational levels in the CN($B^2\Sigma^+$) spectra. Signal due to the CH($A^2\Delta-X^2\Pi$) transition is also observed in the 16 eV energy spectrum, as illustrated by Figure 6a. As is the case with CN($B^2\Sigma^+$), the observed CH($A^2\Delta$) emission is also due to the $\Delta v = 0$ series of transitions. The intense Q branch, as expected in spectra of $^2\Delta-^2\Pi$ transitions,[50] occurs from the (0,0) and (1,1) vibrational bands, with the P and R branches for the same bands extending out from the band origin. The weaker Q branch of the (2,2) vibrational band is also observed at 23,124 $cm^{-1}$, although its associated P and R branches lack intensity and are not readily identifiable. Signals due to the ($B^2\Sigma^--X^2\Pi$) or ($C^2\Sigma^+-X^2\Pi$) transitions in CH are not observed in the 16 eV spectra, even though they are both energetically feasible. From the thermodynamic calculations given in Table 1, it is clear that CN($B^2\Sigma^+$) can only form together with $CH_3$ at $h\nu = 10.2$ and 11.5 eV. However, the CN($B^2\Sigma^+$) signal observed at 16 eV could occur from as many as four dissociation channels; with $CH_3$, CH($X^2\Pi$) + $H_2$, $CH_2$ + H, or CH($A^2\Delta$) + $H_2$. The thermochemical thresholds for these processes are 8.45, 13.10, 13.21, and 15.98 eV, respectively. Therefore, how the partitioning of excess energy affects the resultant dynamics can be explored; this will be covered in more detail later. Furthermore, the CH($A^2\Delta$) fragment can be produced with CN($X^2\Sigma^+$) + $H_2$ at 12.78 eV or CN($B^2\Sigma^+$) + $H_2$ at 15.98 eV. However, formation of either excited radical via the 15.98 eV channel can be disregarded on the basis of thermodynamics; this topic is covered in section 4.4. It is interesting to note that CH($A^2\Delta$) can only be formed with molecular hydrogen, rather than two H atoms, and formation of a H−H bond suggests a more complex dynamical process than simple fragmentation is occurring.

Spectral fitting is achieved by comparison of the data with simulations generated using the LIFBASE 2.0 package.[51] The line positions are determined from the relevant spectroscopic constants and the intensities are computed from Hönl−London factors, the electronic transition moment (which encompasses the Franck−Condon factor), and the rovibrational wavefunction. The populations of individual $v'$ and $K'$ or $J'$ levels are varied iteratively to minimize the difference between the experimental and simulated spectra. This procedure is initiated in the most intense vibrational bands, where less uncertainty exists in the resultant populations. The resultant spectral fits are shown inverted in Figures 3a, 4a, 5a and 6a. To evaluate the accuracy of the spectral fits, the peak correlation (PC) value is calculated for each experimental spectrum/simulation pair by the LIFBASE program using the following expression:[51]

$$PC = \frac{nS_{xy} - S_xS_y}{[(nS_x^2 - S_x^2)(nS_y^2 - S_y^2)]^{0.5}} \quad (1)$$

where $S_x$ and $S_y$ are the summation of all data points in either the simulated or experimental spectra, respectively, $S_{xy}$ is the cross summation of both the simulated and experimental spectra, and $n$ is the number of data points in either spectrum; an interpolation is performed so that $n$ is the same for both spectra. The PC values are ca. 0.95 for all of the fits apart from that of the 10.2 eV spectrum, where the poor signal-to-noise ratio only permits a value of ca. 0.75. Because predissociation distorts the CH($A^2\Delta$) rotational populations in levels higher than $J' = 22$ or 10 for $v' = 0$ or 1, respectively,[52] only populations below these levels are considered. The simulated resolutions that give the best fit to the experimental data are 1.5 and 2 $cm^{-1}$ for the CH($A^2\Delta-X^2\Pi$) and CN($B^2\Sigma^+-X^2\Sigma^+$) spectra, respectively. The CN($B^2\Sigma^+-X^2\Sigma^+$) transition belongs to Hund's case b; therefore the rotational levels of this transition are denoted $K$, whereas those of the CH($A^2\Delta-X^2\Pi$) system are denoted $J$, because this transition is best described by an intermediate regime between the limiting cases of Hund's cases a and b.[50] This notation will be used when each transition or excited-state is explicitly referred to.

Using these fits, determination of the rotational and vibrational populations in the electronically excited fragments is possible. This information permits the subsequent determination of the vibrational temperature ($T_{vib}$) and the rotational temperature ($T_{rot}$) for each radical using Boltzmann plots. The rotational fits for all of the spectra are displayed in Figures 3b, 4b,c, 5b−d, and 6b,c. Scatter in the data is apparent in some of these graphs, especially for the CN($B^2\Sigma^+$, $v' = 2$) plot acquired using $h\nu =$ 16 eV (Figure 5d) because of diminished band intensity. This effect is due to the values of the Franck−Condon factors, which are 0.909, 0.757, 0.649, and 0.574 for the (0,0), (1,1), (2,2),

**TABLE 3: Summary of the Calculated Rotational and Vibrational ($\lambda_v$) and Rotational ($\theta_R$) Surprisal Parameters**

| excited fragment | $h\nu$ (eV) | $T_{vib}$ (K) | $\lambda_v$ | $v'$ | $T_{rot}$ (K) | $\theta_R$[a] | $\theta_R$[b] | $\theta_R$[c] | $\theta_R$ |
|---|---|---|---|---|---|---|---|---|---|
| CN($B^2\Sigma^+$) | 10.2 | | | 0 | (80 ± 40),[e] 1840 ± 500 | 46.4 ± 7.2, 1.9 ± 0.4 | | | |
| | 11.5 | 4700 ± 400 | −4.3[a,d] | 0 | 570 ± 100, 7460 ± 400 | 77.4 ± 16.4, 0.3 ± 0.6 | | | |
| | | | | 1 | 500 ± 70, 5910 ± 400 | 34.6 ± 1.2, 1.4 ± 0.8 | | | |
| | 16 | 5000 ± 600 | −2.1 ± 0.2[a] | 0 | 600 ± 50, 7700 ± 200 | 91.8 ± 21.5, 2.9 ± 1.6 | 14.5 ± 2.7, 2.4 ± 0.8 | 33.1 ± 6.5, 0.6 ± 0.6 | |
| | | | −4.8 ± 1.4[b] | 1 | 440 ± 70, 2725 ± 200 | 59.6 ± 14.7, 9.6 ± 1.3 | 13.6 ± 8.4, 2.2 ± 0.9 | 12.9 ± 3.3, 1.9 ± 0.8 | |
| | | | −2.5[c,d] | 2 | 375 ± 160, 3000 ± 500 | 45.5 ± 7.2, 2.5 ± 0.9 | 8.4,[d] 4.5 ± 1.6 | *f* | |
| CH($A^2\Delta$) | 16 | 5100[d] | −1.1[d] | 0 | 4895 ± 140 | | | | 1.6 ± 0.1 |
| | | | | 1 | 2590 ± 110 | | | | 2.5 ± 0.5 |

[a] The chosen dissociation channel is $CH_3CN \rightarrow CH_3 + CN(B^2\Sigma^+)$, $\Delta H^0_{298} = 8.45$ eV. [b] The chosen dissociation channel is $CH_3CN \rightarrow CH(X^2\Pi) + CN(B^2\Sigma^+) + H_2$, $\Delta H^0_{298} = 13.10$ eV. [c] The chosen dissociation channel is $CH_3CN \rightarrow CH_2 + CN(B^2\Sigma^+) + H$, $\Delta H^0_{298} = 13.21$ eV. [d] No error is presented with this value as it came from a plot comprising two points. [e] The value in brackets is subject to a higher degree of uncertainty due to signal-to-noise constraints. [f] No $\theta_R$ values obtained, as $E_v > E_R$ in prior distribution.

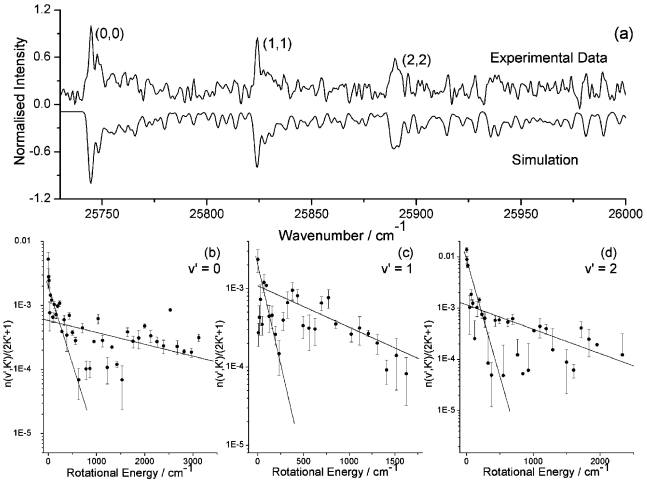


**Figure 5.** (a) Experimental and simulated spectra of the CN($B^2\Sigma^+ - X^2\Sigma^+$) transition resulting from photodissociation of $CH_3CN$ at 16 eV. The simulated spectrum is inverted for clarity. (b)−(d) Boltzmann plots of the rotational populations in the $v' = 0$, 1, or 2 level versus the available rotational energy.

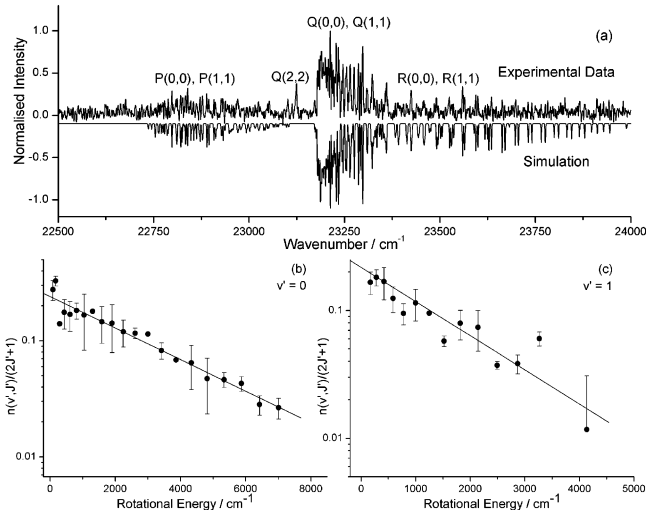


**Figure 6.** (a) Experimental and simulated spectra of the CH($A^2\Delta - X^2\Pi$) transition resulting from photodissociation of $CH_3CN$ at 16 eV. The simulated spectrum is inverted for clarity. (b), (c) Boltzmann plots of the rotational populations in the $v' = 0$ or 1 level versus the available rotational energy.

and (3,3) bands, respectively.[37] The (2,2) and (3,3) bands of the data acquired at $h\nu = 11.5$ eV are too weak for the reliable extraction of populations. Note that the best spectral fits for each spectrum result from some compromises, in that the P branch fits better than the corresponding R (or Q in the case of CH($A^2\Delta$)) branch for some rovibrational lines or vice versa. Therefore, error bars for the plots are obtained by altering the population of a single rotational level to provide the best possible fit for the P line at the expense of the corresponding R (and Q) line and vice versa. In most cases, it is clear from the associated error bars that the uncertainty in the populations at lower values of $K'$ are larger than those at higher $K'$, in agreement with the reduced intensity of the lines near the band origin. All of the CN($B^2\Sigma^+$) plots exhibit a bimodal rotational distribution, although the weak bands at lower $K'$ cast some doubt on the validity of this observation for the 10.2 eV ($v' = 0$) plot, as denoted by a dotted line. A single distribution is observed in both rotational plots obtained from the CH($A^2\Delta$) spectrum at 16 eV. Values for $T_{rot}$ are extracted from the Boltzmann fits, as displayed in Table 3. Where two values are given, the first value is for the distribution at lower $K'$ and the second value corresponds to the distribution at higher $K'$; these values are represented by $T_{rot,low}$ and $T_{rot,high}$ from here onward. A summation of the rotational populations for each $v'$ level gives the relative vibrational populations, with a single value of $T_{vib}$ resulting from each spectrum. This data is also presented in Table 3. It is worth noting that the $T_{rot,high}$ value for CN($B^2\Sigma^+$, $v' = 0$) increases markedly when the photon energy is increased from 10.2 to 11.5 eV but stays approximately constant when $h\nu$ is further increased to 16 eV. In addition, the $T_{vib}$ for CN($B^2\Sigma^+$) produced by 11.5 and 16 eV photons and the CH($A^2\Delta$) formed at $h\nu = 16$ eV are very similar at approximately 5000 K.

**3.3. Surprisal Analysis of Energy Partitioning to Vibrations and Rotations.** One method for analyzing the energy disposal in a photodissociation process is the surprisal analysis, which quantifies the deviation of the measured vibrational or rotational distribution, denoted as $P(v)$ or $P(v,J)$, from the expected prior distribution, $P^0(v)$ or $P^0(v,J)$.[53,54] When the product of interest is a diatomic, $P^0(v)$ is determined from the expression:

$$P^0(v) = \frac{5}{2}(1 - f_v)^{3/2} \quad (2)$$

where $f_v = E_v/E_{xs}$ and $E_v$ is the vibrational energy of each product in vibrational level $v$, summed over all products formed in a given dissociation channel. For a linear diatomic, $E_v = \omega_e(v + (0.5)) - \omega_e x_e(v + 0.5)^2$ where $\omega_e$ is the fundamental frequency of vibration and $\omega_e x_e$ is the anharmonicity term,[50] whereas $E_v = \sum_{i=1}^{s}(v_i + 0.5)\omega_i$ for a nonlinear species, where $s$ is the number of vibrational degrees of freedom.[55] $CH_3$ and $CH_2$ are the only nonlinear molecules considered here, with these moieties possessing six and three vibrational degrees of freedom, respectively. $E_{xs}$ is the excess energy, which is given by ($h\nu$ + thermal energy of $CH_3CN$ − energy of dissociation channel). The thermal energy of acetonitrile is calculated to be 0.06 eV at 298 K from a summation of available rotational and vibrational terms[45] and the appropriate dissociation channel energy is taken from Table 1. Calculations are performed for each of several key product channels, as listed in Table 3. The vibrational surprisal parameters are obtained from the following equation:[53,54]

$$-\ln\left(\frac{P(v)}{P^0(v)}\right) = \lambda_0 + \lambda_v f_v \quad (3)$$

where $\lambda_v$ is the surprisal parameter for vibration and $\lambda_0$ is a normalizing factor. Therefore, a plot of $-\ln(P(v)/P^0(v))$ versus $f_v$ yields a plot with a gradient equal to $\lambda_v$, as seen in Figure 7 for the emission from CN($B^2\Sigma^+$) at 16 eV. A similar analysis can be performed on the rotational populations. The fraction of energy channeled into rotation is given by $g_R = E_R/(E_{xs} - E_v)$, where $E_R$ is the rotational energy of each product in a given rotational level, summed over all products formed in a given dissociation channel. Because both of the nonlinear molecules considered here ($CH_3$ and $CH_2$) are symmetric, each rotational level can be considered to be $(2J + 1)^2$ degenerate, therefore $E_R = BJ(J + 1)$ for these species.[55] The rotational surprisal plot is extracted from

$$-\ln\left(\frac{P(v,J)}{P^0(v,J)}\right) = \lambda_0 + \lambda_v f_v + \theta_R g_R \quad (4)$$

In this instance, $P^0(v,J) \propto (2J + 1)(E_{xs} - E_v - E_R)^{1/2}$ and $\theta_R$ is the rotational analogue of $\lambda_v$. In both methods the actual and prior distributions are normalized so that $\sum P^0 = 1$. Positive values of $\lambda_v$ denote that the observed vibrational distribution is colder than that expected by the prior distribution and vice versa. Similar trends for the rotational distributions can be indicated from the sign of the derived $\theta_R$ values. The extracted values for both $\lambda_v$ and $\theta_R$ are listed in Table 3. Only one dissociation channel is possible for production of CN($B^2\Sigma^+$) to occur at $h\nu$ = 10.2 and 11.5 eV (the CN($B^2\Sigma^+$) + $CH_3$ channel, $\Delta H^0_{298}$ = 8.45 eV) or for CH($A^2\Delta$) production at $h\nu$ = 16 eV (CH($A^2\Delta$) + CN($X^2\Sigma^+$) + $H_2$, $\Delta H^0_{298}$ = 12.78 eV). However, three different dissociation channels can form CN($B^2\Sigma^+$) when 16 eV photons are used; CN($B^2\Sigma^+$) + $CH_3$, CN($B^2\Sigma^+$) + CH($X^2\Pi$) + $H_2$, or CN($B^2\Sigma^+$) + $CH_2$ + H. The thermochemical thresholds of these channels are 8.45, 13.10, or 13.21 eV, respectively. Therefore, the values for the vibrational and rotational surprisal parameters for production of CN($B^2\Sigma^+$) at 16 eV will be calculated for each of the three possible dissociation channels; these are displayed as three values in column 4 and the numbers in columns 7−9 of Table 3. All of the $\lambda_v$ values for both fragments are negative, thereby indicating that a greater than statistical proportion of the excess energy goes into vibration.

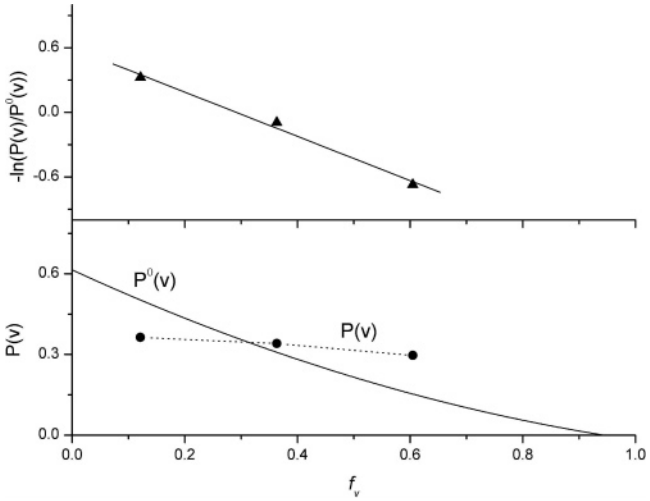


**Figure 7.** Vibrational surprisal plot from the CN($B^2\Sigma^+ - X^2\Sigma^+$) emission observed at 16 eV, where the chosen dissociation channel is $CH_3CN \rightarrow CH_3$ + CN($B^2\Sigma^+$) ($\Delta H^0_{298}$ = 8.45 eV). The gradient of the linear fit in the upper portion corresponds to $\lambda_v = -2.1 \pm 0.2$.

No clearly discernible trend can be determined when the chosen dissociation channel for CN($B^2\Sigma^+$) at 16 eV is varied. The $\theta_R$ values for CN($B^2\Sigma^+$) are all bimodal at 10.2, 11.5, and 16 eV, with the values corresponding to the lower rotational distribution being appreciably colder than predicted by the prior distribution. On the contrary, the rotational surprisal parameters obtained for the higher rotational distribution are approximately zero in all cases; thus the rotational distributions from which they are derived are nearly statistical.

**3.4. CH($A^2\Delta$)/CN($B^2\Sigma^+$) Ratio at 16 eV.** The relative ratio of CH($A^2\Delta$)/CN($B^2\Sigma^+$) produced at 16 eV can be calculated using the procedure of Sorkhabi et al., fully described elsewhere.[56] The population of rotational state $J'$ of a vibrational state $v'$ in an excited electronic state $\Lambda'$ is denoted $N(\Lambda',v',J')$ and is given by the following expression for a bimodal rotational distribution:

$$N(\Lambda',v',J') = (2J' + 1)[A_1 e^{-\Delta E_{J'}/k_B T_{rot,low}} + A_2 e^{-\Delta E_{J'}/k_B T_{rot,high}}] \quad (5)$$

where $A_x$ is a constant for a given vibrational band, $\Delta E_{J'}$ is the energy of a given rotational level, and $T_{rot,low}$ and $T_{rot,high}$ are taken from the experimental Boltzmann fits. Although this expression is formulated for a bimodal rotational distribution, it can also be used for a population exhibiting a single population distribution. Using the calculated $N(\Lambda',v',J')$ values in eq 6, whose full derivation is stated in ref 56, gives the relative ratio of CH($A^2\Delta$)/CN($B^2\Sigma^+$):

$$\frac{N_T(\mathrm{CH}(A^2\Delta))}{N_T(\mathrm{CN}(B^2\Sigma^+))} = \frac{N(\mathrm{CH}(A^2\Delta),v',J')}{N(\mathrm{CN}(B^2\Sigma^+),v',K')} \frac{P_{J'}(\mathrm{CN}(B^2\Sigma^+))}{P_{J'}(\mathrm{CH}(A^2\Delta))} \frac{P_{v'}(\mathrm{CN}(B^2\Sigma^+))}{P_{v'}(\mathrm{CH}(A^2\Delta))} \frac{S_{v'v''}(\mathrm{CN}(B^2\Sigma^+))}{S_{v'v''}(\mathrm{CH}(A^2\Delta))} \quad (6)$$

where $N_T(\Lambda')$ is the total population of electronic state $\Lambda'$, $P_{J'}(\Lambda')$, and $P_{v'}(\Lambda')$ are probabilities of being in state $J'$ and $v'$ of electronically excited state $\Lambda'$, respectively. $P_{J'}(\Lambda')$ is calculated by determining $N(\Lambda',v',J')$ using eq 5 and dividing by the sum of all $N(\Lambda',v',J')$ values for a particular $v'$ level. $P_{v'}(\Lambda')$ is determined from a modified Boltzmann equation using the $T_{vib}$ values determined from the experimental data.

$S_{v'v''}(\Lambda')$ is the band strength of a transition between the vibrational levels $v'$ and $v''$ in an excited electronic state $\Lambda'$ that is given by[57]

$$S_{v'v''}(\Lambda') = \bar{R}_e^{\,2} q_{v'v''} \tag{7}$$

where $\bar{R}_e^{\,2}$ and $q_{v'v''}$ are the average electronic transition moment and the Franck−Condon factor, respectively, for the selected band. Incorporation of $S_{v'v'}(\Lambda')$ into eq 6 permits scaling of the data derived from the CH($A^2\Delta-X^2\Pi$) and CN($B^2\Sigma^+-X^2\Sigma^+$) spectra. Values of $\bar{R}_e^2$ and $q_{v'v'}$ for the (0,0) and (1,1) bands of the CH($A^2\Delta-X^2\Pi$) and CN($B^2\Sigma^+-X^2\Sigma^+$) transitions are taken from the literature.[37,52,58,59] Using this method, the ratio $N_T(CH(A^2\Delta))/N_T(CN(B^2\Sigma^+))$ is independent of the rotational levels or vibrational bands chosen, so that any permutation of $N(CH(A^2\Delta),v',J')$ and $N(CN(B^2\Sigma^+),v',K')$ should produce the same result for the electronic ratio.[56] This internal check proves to be correct, resulting in a CH($A^2\Delta$)/CN($B^2\Sigma^+$) ratio of (1.2 ± 0.1):1 at $h\nu = 16$ eV. The error bars are derived by inputting the experimentally derived $T_{vib}$ and $T_{rot}$ values plus or minus their associated error to give the maximum or minimum final ratio value.

## 4. Discussion

**4.1. Origin of Observed CH($A^2\Delta-X^2\Pi$) and CN($B^2\Sigma^+-X^2\Sigma^+$) Emission.** To investigate the photodissociation mechanism of $CH_3CN$, the nascent vibrational and rotational distributions are used. The following section details considerations related to the origin of the observed emission signals. Excitation occurs to Rydberg levels that correlate with dissociation products via unbound states when using 10.2 or 11.5 eV photons.[14,33] Using either of these photon energies, only the $B^2\Sigma^+$ excited state of the CN fragment can be directly accessed (see Tables 1 and 2). Therefore, the observed CN($B^2\Sigma^+-X^2\Sigma^+$) emission using 10.2 or 11.5 eV photons is not from relaxation of higher excited electronic states. Superexcited states of $CH_3CN$ are accessed using a 16 eV photon.[60] States of this type lie above the ionization potential of the molecule and lead to either ionization or dissociation into neutral fragments. Previous work has proposed that excitation of acetonitrile with $h\nu > 13$ eV leads to the formation of superexcited $CH_3CN^{**}$, which subsequently dissociates to form highly excited diatomic products.[33,34] A cascade of relaxation from higher excited states of CN** or CH** would cause enhancement of population in the CN($B^2\Sigma^+$) and CH($A^2\Delta$) states, therefore resulting in non-nascent rotational or vibrational distributions in either excited radical. From the selection rule for electronic transitions of $\Delta\Lambda = 0, \pm 1$,[50] the only allowed transitions to the experimentally observed states are from the $D^2\Pi$, $E^2\Sigma^+$, $G^2\Pi$, or $H^2\Pi$ states for the CN fragment and the $D^2\Pi$ or $E^2\Pi$ states in the case of CH. It is clear from Table 2 that $h\nu > 17.40$ eV is required to access either the $D^2\Pi$ or $E^2\Pi$ levels of CH. Therefore, the CH($A^2\Delta-X^2\Pi$) signal we observe from dissociation at 16 eV results from direct population of the CH($A^2\Delta$) state. For CN it is energetically possible to reach the highly excited states that can relax down to the $B^2\Sigma^+$ state with $CH_3$ as the partner fragment. However, when one considers that hydrogen atom removal is a facile process that can occur at relatively low VUV photon energies (see Table 1 and ref 61), it is apparent that this assignment of partner fragment is not certain. Therefore, if the the more plausible $CH_2$ or CH fragments are taken as the coproduced species, the threshold for population of electronic states higher than $B^2\Sigma^+$ of CN is 16.66 eV, too high in energy to be reached by a 16 eV photon. Thus, the CN($B^2\Sigma^+-X^2\Sigma^+$) signal at 16 eV is likely to occur from direct population of the CN($B^2\Sigma^+$) state.

To know that the observed emissions are truly due to nascent distributions, one has to prove that the excited products do not undergo collisions prior to radiative relaxation. Confirmation that the data is from the nascent regime is especially important when considering bimodal distributions, because the observation of two distinct $T_{rot}$ values could be due to collisional deactivation of the initial products, which would relax a portion of the excited population into lower rotational levels. In recent studies performed on this apparatus, calculations found that >98% of the excited state CH* emission occurs from species that have not participated in any collisions at $P = 20$ Pa.[7,41] Given that the emission lifetime of CN($B^2\Sigma^+$) is ≈7.5 times shorter than that of CH($A^2\Delta$) (72 ns vs 537 ns)[62,63] and the operating pressure here is ≈9 Pa, the populations derived from the fluorescence of both of these electronically excited radicals can be considered to be nascent.

**4.2. CN($B^2\Sigma^+-X^2\Sigma^+$) Emission Observed at $h\nu = 10.2$ eV.** Using the calculated energetics given in Table 1, the emission observed from CN($B^2\Sigma^+$) at 10.2 eV could only occur when $CH_3$ is the partner fragment. Population of CN($B^2\Sigma^+$) vibrational levels up to $v' = 6$ is energetically possible if all of the excess energy goes to the excited CN* fragment, because there is 1.68 eV of excess energy ($E_{xs}$ − vibrational excitation in CN($B^2\Sigma^+$)). Only the (0,0) band is observed in the 10.2 eV spectrum presented here, which would indicate that the CN($B^2\Sigma^+$) fragment is produced with population in only $v' = 0$ using a Lyman-α photon. Suppression of the vibrational excitation in CN($B^2\Sigma^+$) has been observed before due to partitioning of energy to the $CH_3$ moiety.[38] However, the result reported here is contrary to that found by two previous studies using photon energies near 10.2 eV, with population up to $v' = 2$ and 3 reported by Ashfold and Simons and Moriyama et al., respectively.[36,37] Therefore, one must conclude that the signal-to-noise in our spectrum presented in Figure 3a is too limited and any conclusions derived from this data should be treated with this caveat in mind. This constraint can be attributed to the weak overall signal at this photon energy, supported by the action spectrum given in Figure 1, which only permits data collection when the beam current of the storage ring is near its peak of ca. 400 mA. The rotational surprisal for lower $K'$ levels for $v' = 0$ is colder than expected from the prior distribution, whereas the surprisal nearly matches the expected distribution when higher $K'$ levels are populated. These observations suggest that the fragmentation mechanism may occur from a linear symmetric configuration on a time scale approaching that of an impulsive dissociation for the lower rotational levels. As the extent of rotational excitation increases, however, $CH_3CN$ fragmentation may occur from a bent transition state or over a longer time, which is more indicative of a statistical partitioning of the excess energy into rotations. The bimodal rotational distribution observed when $h\nu = 10.2$ eV supports the previous work of Ashfold and Simons, rather than the single distribution found by Moriyama et al. [36,37] Furthermore, the rotational distribution at higher $K'$ corresponds to a $T_{rot,high}$ value of 1840 ± 500 K, whereas Moriyama et al. derived a temperature of 8000 K. This might be due to the low resolution of their spectrum (ca. 13 $cm^{-1}$), where individual rotational lines are impossible to distinguish. The low signal-to-noise in our spectrum might also be a factor in this discrepancy, but the data points used to obtain $T_{rot,high}$ correspond to rotational levels in the region of the intense P band head. Ashfold and Simons

explained their bimodal distributions using the intuitive scheme that dissociation from a linear excited configuration leads to lower rotational product excitation than dissociation originating in a bent state.[36] Thus, there is a transition from a linear excited electronic state to a bent excited state. A bimodal pattern is supported by the derived rotational surprisal parameters, and it is likely that this mechanism can also be used to explain our observations.

**4.3. CN($B^2\Sigma^+-X^2\Sigma^+$) Emission Observed at $h\nu = 11.5$ eV.** Kanda et al. observed CN($B^2\Sigma^+-X^2\Sigma^+$) emission from the reaction of metastable Ar($^3P_2$) atoms with $CH_3CN$ in a flowing afterglow.[38] The excitation energy in this case equals the internal energy of the argon atoms (11.548 eV). Therefore, the $T_{rot}$ values derived here from the 11.5 eV data can be compared to those reported by Kanda et al. They observed bimodal rotational distributions up to $v' = 4$ and obtained values of $T_{rot,low}$ similar to those obtained here.[38] However, their $T_{rot,high}$ values are ca. 1600 and 1900 K lower than ours for $v' = 0$ and 1, respectively, which equate to differences in rotational excitation of 0.14 and 0.16 eV. These discrepancies might be attributed to the collision energy employed in the flowing afterglow study. Emission from CN($B^2\Sigma^+$) using 11.5 eV photons can only occur when $CH_3$ is the coproduct, resulting in an excess energy of 3.11 eV. Therefore, because excitation to CN($B^2\Sigma^+$, $v' = 3$) is observed in our work, accounting for 0.91 eV, there is an additional 2.20 eV available for rotational excitation of CN($B^2\Sigma^+$) and internal modes of the methyl group. This is insufficient energy for electronic excitation to the $CH_3(^2A_1')$ state, although the excitation of multiple quanta of vibrational and rotational modes could occur in the $CH_3$ fragment. The derived negative value of $\lambda_v$ for CN($B^2\Sigma^+$) at 11.5 eV indicates that this fragment is vibrationally hotter than expected, thus indicating that the transfer of excess energy into the C≡N vibration is efficient. As with the data acquired at 10.2 eV, the $\theta_R$ values show a significantly colder than predicted distribution at lower $K'$ and nearly similar to statistical energy partitioning at higher $K'$. These data signify that fragmentation arises from a linear transition state at lower $K'$ of CN($B^2\Sigma^+$) on a time scale indicative of impulsive dissociation. This geometry confers a lesser extent of rotational torque to the departing CN($B^2\Sigma^+$) moiety than predicted. In contrast, the higher $K'$ states occur via a bent transition state, which can provide rotational excitation to the CN($B^2\Sigma^+$) fragment formed in the dissociation process. The agreement between the pattern observed at high $K'$ and the surprisal prediction indicates that this process occurs on a time scale long enough for statistical energy partitioning to occur in the CN($B^2\Sigma^+$) product.

**4.4. CN($B^2\Sigma^+-X^2\Sigma^+$) and CH($A^2\Delta-X^2\Pi$) Emission Observed at $h\nu = 16$ eV.** The observation of dual emission from the CH($A^2\Delta$) and CN($B^2\Sigma^+$) excited states at a photon energy of 16 eV warrants further discussion. Both of these emissions can either be caused by the same photolysis event or occur via competing dissociation channels. According to Table 1, both of these electronically excited radicals can be produced simultaneously in their ground vibrational levels together with a hydrogen molecule when $h\nu = 15.98$ eV is used. Assignment of the vibrational bands in Figure 5a reveals that the $v' = 3$ level of CN($B^2\Sigma^+$) is populated, which requires an additional 0.91 eV to be deposited. Similarly, the CH($A^2\Delta$) excited radical is populated up to the $v' = 2$ level, as seen in Figure 6a; thus an additional 0.83 eV of vibrational energy is imparted to this fragment. As there would only be an excess energy of 0.02 eV available at 16 eV if the 15.98 eV channel is accessed, these fragments can most likely only be formed in such vibrationally excited states in separate photodissociation events. It may be possible to produce CN($B^2\Sigma^+$) in conjunction with $CH_3$ at $h\nu = 16$ eV. If the methyl group were formed with considerable internal excitation, subsequent unimolecular fragmentation could form CH($A^2\Delta$) and may give the impression of simultaneous production of both electronically excited diatomics. Considering the $CH_3$ + CN($B^2\Sigma^+$) channel ($\Delta H^0_{298} = 8.45$ eV), the internal energy of the $CH_3CN$ parent molecule at 298 K (0.06 eV) and the extent of vibrational excitation in CN($B^2\Sigma^+$) observed in the 16 eV spectrum (Figure 5a), $E_{xs}$ equals 6.70 eV for this channel. Previous studies of the photodissociation of $CH_3$ show that at least 7.55 eV is required for the $CH_3 \rightarrow CH(A^2\Delta) + H_2$ process to occur.[64] Therefore, there is insufficient energy available to form CH($A^2\Delta$) by this two step mechanism at $h\nu = 16$ eV, thus requiring the formation of either CH($A^2\Delta$) or CN($B^2\Sigma^+$) by separate dissociation processes at this photon energy.

Production of the excited CN($B^2\Sigma^+$) can form in conjunction with either $CH_3$, CH($X^2\Pi$) + $H_2$ or $CH_2$ + H at or above thermochemical thresholds of 8.45, 13.10, or 13.21 eV, respectively. Relative to the photon energy of 16 eV, these channels show a range of different excess energies that can be partitioned into the various product vibrational and rotational modes. If the observed degree of vibrational excitation of CN($B^2\Sigma^+$) is considered, the excess energies are 6.70, 2.05 and 1.94 eV, respectively. One would naturally expect the vibrational excitation to increase as the available excess energy also increases. However, this trend is not observed in the $\lambda_v$ data obtained from the 16 eV CN($B^2\Sigma^+$) emission spectrum (see Table 3). The CN($B^2\Sigma^+$) + $CH_3$ and CN($B^2\Sigma^+$) + $CH_2$ + H channels exhibit the same extent of vibrational excitation relative to their respective prior distributions, which is more excited than the forecast. These observations could be rationalized by considering the total number of vibrational degrees of freedom (denoted $s$) in the products formed by each of these channels. Although the CN($B^2\Sigma^+$) + $CH_3$ channel has a much larger amount of excess energy than the CN($B^2\Sigma^+$) + $CH_2$ + H channel (6.70 eV vs 1.94 eV), the products of the former pathway have a total $s$ value of 7, compared to a total $s$ of 4 in the latter case. Therefore, the excess energy is spread over more modes in the former case, thereby accounting for more of the excess energy than in the latter channel. However, excitation of one quanta in each of the additional modes would only equal a total of ca. 1 eV, so other processes must be considered. Because all of the rotational surprisal parameters for CN($B^2\Sigma^+$) at 16 eV are positive, these rotational distributions are colder than expected and cannot explain the similarity in $\lambda_v$ for both of these channels. Therefore, the excess energy is most probably apportioned into the translational kinetic energies of the fragments. The $\lambda_v$ value for the CN($B^2\Sigma^+$) + CH($X^2\Pi$) + $H_2$ channel is ca. twice that of the other potential pathways. Because both the total $s$ value for the coproducts and the $\Delta H^0_{298}$ of this channel are very close to those for the CN($B^2\Sigma^+$) + $CH_2$ + H pathway, this disparity is surprising. This comparison indicates that formation of diatomic coproducts results in significantly more vibrational excitation in CN($B^2\Sigma^+$) compared to when polyatomic partner species are formed. In accord with the results for the CN($B^2\Sigma^+$) fragment at other photon energies, the $\theta_R$ values show a significantly colder than predicted partitioning at lower $K'$ and a similar to statistical rotational energy allocation at higher $K'$, regardless of the partner fragments. Another potential pathway to form the various $CH_x$ partner species is the initial production of $CH_3^*$ + CN($B^2\Sigma^+$). The methyl radical can subsequently dissociate into either CH($X^2\Pi$) + $H_2$ or $CH_2$ + H if it is formed

with substantial internal excitation; at least 4.65 or 4.76 eV, respectively, is required to form either pair of products listed above from $CH_3$. Because the formation of $CH_3 + CN(B^2\Sigma^+, v' = 3)$ from $CH_3CN$ using a 16 eV photon results in an excess energy of 6.70 eV, this two-step mechanism is also possible.

The $CH(A^2\Delta)$ produced at 16 eV can only occur in conjunction with $CN(X^2\Sigma^+) + H_2$, thereby indicating an excess energy of 2.45 eV when the observed vibrational excitation to $v' = 2$ is included. From the derived surprisal parameters, it can be seen that an increase in the partitioning of excess energy into vibration is observed and the $\theta_R$ values for both $v' = 0$ and 1 exhibit an approximately statistical allocation of energy into rotation. These data suggest that transfer of excess energy into vibration is more efficient than to rotational modes of the products. It is also possible that part of the excess energy is apportioned to electronic excitation of the partner CN fragment to its first excited electronic state ($A^2\Pi$), which is 1.14 eV above the ground state of CN. However, as this state emits in the near IR spectral region it is not detected in this experiment. The formation of molecular hydrogen in the $CH(A^2\Delta) + CN(X^2\Sigma^+) + H_2$ channel is interesting, because formation of this product could occur either via concerted breaking of two C−H bonds or through a two step mechanism, where very highly excited $CH_3$* and ground state $CN(X^2\Sigma^+)$ are initially formed. For the latter pathway, the formation of $CH_3 + CN(X^2\Sigma^+)$ results in an excess energy of 10.80 eV when $h\nu = 16$ eV, because $\Delta H^0_{298} = 5.26$ eV to form these products. The predissociation of high-lying Rydberg levels of $CH_3$* into $CH(A^2\Delta) + H_2$ has been detected elsewhere.[64] The thermodynamic threshold for forming $CH(A^2\Delta, v' = 2) + H_2$ from the methyl radical is calculated as 8.38 eV from the minimum photon energy to give $CH(A^2\Delta)$ signal from $CH_3$ in the previous study (7.55 eV)[64] plus the 0.83 eV required to populate $CH(A^2\Delta)$ up to the $v' = 2$ level. Therefore, the two-step mechanism is viable if a substantial portion of the excess energy is partitioned into the methyl fragment. Another possibility for forming molecular hydrogen is the liberation of one hydrogen atom, which then abstracts an additional H from the residual $CH_2CN$ or $CH_2$ moiety. This mechanism is reminiscent of the "roaming" atom scheme in formaldehyde, whose experimental signature is the formation of vibrationally excited $H_2(v = 6-8)$.[27−30] Positive identification of this pathway would provide additional evidence for a new class of dynamics that is not fully described using conventional transition state theory. Because $CH_3CN$ has very similar molecular connectivity and size to $CH_3CHO$, where related features have recently been seen,[30] this argument does seem plausible. Furthermore, the molecular hydrogen created by such a process must be born with 2.91−3.55 eV of excess energy for the $v = 6-8$ vibrational levels of $H_2$ to be populated. Formation of vibrationally excited $CH(A^2\Delta, v' = 2)$, observed in this work, alongside ground state $CN(X^2\Sigma^+)$ and $H_2$ from $CH_3CN$ at $h\nu = 16$ eV results in $E_{xs} = 2.45$ eV. As a consequence, any $H_2$ produced in this experiment would experience reduced, but similar, vibrational excitation with respect to that formed in previous examples of the "roaming" atom mechanism. Alas, the experiments performed here are insufficient to determine which fragmentation process is occurring; further studies are required to confirm the dissociation mechanism for this channel.

At 16 eV, dissociation could occur via states of the parent ion $CH_3CN^+$. A 16 eV photon is significantly more energetic than the ionization potential of $CH_3CN$ at 12.20 eV, and the quantum yield for ionization is empirically estimated to be ca. 0.85 near 16 eV.[65] However, thermodynamics indicate that there is insufficient energy to form either excited CN* or CH* fragments with ionic partners:[45,66]

$$CH_3CN + h\nu \rightarrow CH_3^+ + CN(B^2\Sigma^+) \qquad \Delta H^0_{298} = 18.28 \text{ eV}$$

$$CH_3CN + h\nu \rightarrow HCNH^+ + CH(A^2\Delta) \quad \Delta H^0_{298} = 18.09 \text{ eV}$$

Furthermore, a comparison of the cross section for production of $CH_3^+$ from $CH_3CN$ by a 15.6 eV photon ($0.1 \times 10^{-18}$ cm$^2$) with the total absorption cross section for $CH_3CN$ at the same energy ($43 \times 10^{-18}$ cm$^2$) gives a branching ratio for $CH_3^+$ formation of only ≈0.2%.[33,34] Because the fluorescence quantum yields for $CN(B^2\Sigma^+ - X^2\Sigma^+)$ and CH* (from $CH_4$) at 16 eV are 10% and ≈5%, respectively,[33,67] it is implausible that either $CN(B^2\Sigma^+ - X^2\Sigma^+)$ or $CH(A^2\Delta - X^2\Pi)$ emission is occurring in conjunction with ionization in a single photon event. Once again, the $T_{rot}$ data derived from the 16 eV spectrum can be compared to reactions in a flowing afterglow performed elsewhere,[39] although this time the reactive argon species is $Ar^+$. The available energy that $Ar^+$ can impart to $CH_3CN$ equals the energy released when the ion is neutralized (its recombination energy), which is the inverse of the ionization energy, 15.76 eV.[45] Emission from $CH(A^2\Delta - X^2\Pi)$ has been observed in such environments, with the resulting $T_{rot}$ values agreeing well with those observed in this work.[39]

**4.5. CH($A^2\Delta$)/CN($B^2\Sigma^+$) Ratio at 16 eV.** At a photon energy of 16 eV, competition occurs between the channels that form the excited $CH(A^2\Delta)$ and $CN(B^2\Sigma^+)$ fragments. A measure of the relative prominence of these channels can be obtained by calculating the ratio between these two fragments. The derived value of the $CH(A^2\Delta)/CN(B^2\Sigma^+)$ ratio of (1.2 ± 0.1):1 at 16 eV, which approaches the expected stoichiometric ratio of one alkyl and one cyano fragment produced per photon. However, as it has already been established earlier in this article that these processes most probably occur from separate photolysis events, this value indicates that formation of the $CH(A^2\Delta)$ radical has prominence over $CN(B^2\Sigma^+)$ production at 16 eV. This preference is somewhat unexpected from a mechanistic perspective, as formation of the $CN(B^2\Sigma^+)$ radical requires fission of the C−C bond, whereas cleavage of two C−H bonds is additionally required to form $CH(A^2\Delta)$. According to the relative energetics given in Table 1, the C−C single bond is broken in favor of the C≡N triple bond. If this is the case in all dissociation channels accessible with a 16 eV photon, then an alkyl fragment will always be produced in conjunction with a cyano fragment. This interdependence means that one would expect an *overall* $CH_x$:CN ratio of ca. 1:1 (including ground and excited-state species) at this photon energy. Therefore, it is anticipated that photodissociation of $CH_3CN$ at 16 eV could have an equal impact on the hydrocarbon and nitrile chemical schemes that occur in the atmosphere of Titan. This result is consistent with the behavior at lower photon energies, where cleavage of the C−C single bond to form $CH_3$ and CN fragments occurs with unit efficiency,[18] thereby giving a ratio of the ground state $CH_3$:CN fragments of 1:1. The $CH_3$ partner product may be replaced by CH at higher photon energies as some of the extra photon energy is channeled into hydrogen elimination. Photolysis of $CH_3CN$ at 16 eV is possible in the upper atmosphere, where neutral dissociation of nitrile species has been credited a bigger role than that of methane,[18] although this is a minor process relative to ionization of nitrogen. This ratio may have more significance in the interstellar medium, especially in diffuse interstellar clouds. In this instance, higher photon energies can penetrate into the cloud and dissociate $CH_3CN$.[14,15]

## 5. Conclusions

The rotationally resolved spectra of CN($B^2\Sigma^+ - X^2\Sigma^+$) emission obtained by exciting $CH_3CN$ with 10.2, 11.5, and 16 eV photons are presented. All of the derived rotational Boltzmann plots exhibit a bimodal distribution. The results for the lower temperature distribution, i.e., when CN($B^2\Sigma^+$) is only populated in rotational levels with low $K'$, suggests that dissociation occurs from a linear transition state. The colder than predicted rotational distributions in this case suggest a non-statistical fragmentation process occurs, in accordance with dissociation from repulsive potentials.[14,33] However, when CN($B^2\Sigma^+$) experiences further rotational excitation at higher $K'$ values, a similar to statistical partitioning of the rotational energy, combined with much higher rotational temperatures, suggests that a bent transition state is likely in these cases. Such a mechanism has been proposed for photodissociation of ICN, where the states leading to both channels were determined to be linear and bent, respectively.[68−70] This mechanism also agrees with that of Ashfold and Simons for $CH_3CN$.[36] The spectrum of emission from the CH($A^2\Delta - X^2\Pi$) transition at $h\nu = 16$ eV is also obtained. Thermochemical calculations provide credence for the possible coproduction of CN($A^2\Pi$), but this is not observed here. A single distribution is observed in the rotational Boltzmann plot, thereby indicating that the mechanism for disposal of excess energy is consistent for the rotational levels populated. Thus, the excited electronic state that is correlated to the CH($A^2\Delta$) + CN($X^2\Sigma^+$) + $H_2$ fragments is not significantly perturbed by other states. Furthermore, the coproduction of molecular hydrogen opens up the possible occurrence of the "roaming" atom mechanism in highly excited transition states, although a two step mechanism via excited $CH_3^*$ + CN($X^2\Sigma^+$) is also feasible. Further experimental and theoretical studies are required to prove which mechanism occurs when $CH_3CN$ is photodissociated using higher energy VUV photons. There is competition between the formation of CH($A^2\Delta$) and CN($B^2\Sigma^+$) at 16 eV, which coincides with broad features in both the action and absorption spectra (see Figure 1 and ref 33). Several overlapping states may contribute to these peaks and could lead to a multitude of different pathways to the dissociation products. The derived ratio of (1.2 ± 0.1):1 for the CH($A^2\Delta$):CN($B^2\Sigma^+$) excited fragments at 16 eV suggests that production of the former excited fragment is slightly favored at this photon energy, in spite of the extensive rearrangement involved.

**Acknowledgment.** We thank Mike Jimenez-Cruz, Kevin Wilson, and Darcy Peterka of the Chemical Dynamics beamline for their valuable assistance. This work has been supported by the U.S. Department of Energy under contract #DE-AC02-05CH11231. Additional support was provided by the National Aeronautics and Space Administration by grant #NNG06GF26G.

## References and Notes

(1) Miller, J. A.; Bowman, C. *Prog. Energy Combust. Sci.* **1989**, *15*, 287 and references therein.
(2) Casavecchia, P.; Balucani, N.; Cartechini, L.; Capozza, G.; Bergeat, A.; Volpi, G. G. *Faraday Discuss.* **2001**, *119*, 27.
(3) Holzinger, R.; Jordan, A.; Hansel, A.; Lindinger, W. *J. Atmos. Chem.* **2001**, *38*, 187.
(4) Chikan, V.; Nizamov, B.; Leone, S. R. *J. Phys. Chem. A* **2004**, *108*, 10770.
(5) Chikan, V.; Leone, S. R. *J. Phys. Chem. A* **2005**, *109*, 10646.
(6) Elsamra, R. M. I.; Vranckx, S.; Carl, S. A. *J. Phys Chem. A* **2005**, *109*, 10287.
(7) Arrowsmith, A. N.; Chikan, V.; Leone, S. R. *J. Phys. Chem. A* **2006**, *110*, 7521.
(8) Garland, N. L.; Crosley, D. R. *Appl. Opt.* **1985**, *24*, 4229.
(9) Williams, S.; Green, D. S.; Sethuraman, S.; Zare, R. N. *J. Am. Chem. Soc.* **1992**, *114*, 9122.
(10) Thoman, J. W.; McIlroy, A. *J. Phys. Chem. A* **2000**, *104*, 4953.
(11) Luque, J.; Jeffries, J. B.; Smith, G. P.; Crosley, D. R.; Walsh, K. T.; Long, M. B.; Smooke, M. D. *Combust. Flame* **2000**, *122*, 172.
(12) Dalgarno, A.; Black, J. H. *Rep. Prog. Phys.* **1976**, *39*, 573.
(13) Bezard, B.; Marten, A.; Paubert, G. *Bull. Am. Astron. Soc.* **1993**, *25*, 1100.
(14) Suto, M.; Lee, L. C. *J. Geophys. Res.—Atmos.* **1985**, *90*, 3037.
(15) Lee, L. C. *Astrophys. J.* **1984**, *282*, 172.
(16) Hoobler, R. J.; Leone, S. R. *J. Geophys. Res.—Planet.* **1997**, *102*, 28717.
(17) Herbst, E. *Chem. Soc. Rev.* **2001**, *30*, 168.
(18) Wilson, E. H.; Atreya, S. K. *J. Geophys. Res.—Planet.* **2004**, *109*, E06002.
(19) Wilson, E. H.; Atreya, S. K. *Planet. Space Sci.* **2003**, *51*, 1017.
(20) Lebonnois, S.; Bakes, E. L. O.; McKay, C. P. *Icarus* **2002**, *159*, 505.
(21) Israel, G.; Szopa, C.; Raulin, F.; Cabane, M.; Niemann, H. B.; Atreya, S. K.; Bauer, S. J.; Brun, J. F.; Chassefiere, E.; Coll, P.; Conde, E.; Coscia, D.; Hauchecorne, A.; Millian, P.; Nguyen, M. J.; Owen, T.; Riedler, W.; Samuelson, R. E.; Siguier, J. M.; Steller, M.; Sternberg, R.; Vidal-Madjar, C. *Nature* **2005**, *438*, 796.
(22) Vuitton, V.; Yelle, R. V.; Anicich, V. G. *Astrophys. J.* **2006**, *647*, L175.
(23) Ricca, A.; Bauschlicher, C. W.; Bakes, E. L. O. *Icarus* **2001**, *154*, 516.
(24) Hudgins, D. M.; Bauschlicher, C. W.; Allamandola, L. J. *Astrophys. J.* **2005**, *632*, 316.
(25) (a) Allamandola, L. J.; Tielens, A. G. G. M.; Barker, J. R. *Astrophys. J. Suppl. S.* **1989**, *71*, 733 and references therein. (b) Allamandola, L. J.; Hudgins, D. M.; Sandford, S. A. *Astrophys. J.* **1999**, *511*, L115.
(26) Williams, D. *Faraday Discuss.* **2006**, *133*, 449.
(27) Townsend, D.; Lahankar, S. A.; Lee, S. K.; Chambreau, S. D.; Suits, A. G.; Zhang, X.; Rheinecker, J.; Harding, L. B.; Bowman, J. M. *Science* **2004**, *306*, 1158.
(28) Lahankar, S. A.; Chambreau, S. D.; Townsend, D.; Suits, F.; Farnum, J.; Zhang, X. B.; Bowman, J. M.; Suits, A. G. *J. Chem. Phys.* **2006**, *125*, 044303.
(29) Marcy, T. P.; Diaz, R. R.; Heard, D.; Leone, S. R.; Harding, L. B.; Klippenstein, S. J. *J. Phys. Chem. A* **2001**, *105*, 8361.
(30) Houston, P. L.; Kable, S. H. *P. Natl. Acad. Sci. U.S.A.* **2006**, *103*, 16079.
(31) Nuth, J. A.; Glicker, S. *J. Quant. Spectrosc. Radiat. Transfer* **1982**, *28*, 223.
(32) Eden, S.; Limao-Vieira, P.; Kendall, P.; Mason, N. J.; Hoffmann, S. V.; Spyrou, S. M. *Euro. Phys. J. D* **2003**, *26*, 201.
(33) Kanda, K.; Nagata, T.; Ibuki, T. *Chem. Phys.* **1999**, *243*, 89.
(34) Mitsuke, K.; Mizutani, M. *J. Electron Spectrosc. Rel. Phenom.* **2001**, *119*, 115.
(35) Cody, R. J.; Dzvonik, M. J.; Glicker, S. *J. Chem. Phys.* **1985**, *82*, 3100.
(36) Ashfold, M. N. R.; Simons, J. P. *J. Chem Soc. Farad. Trans. 2* **1978**, *74*, 1263.
(37) Moriyama, M.; Tsutsui, Y.; Honma, K. *J. Chem Phys.* **1998**, *108*, 6215.
(38) Kanda, K.; Igari, N.; Kikuchi, Y.; Kishida, N.; Igarashi, J.; Katsumata, S.; Suzuki, K. *J. Phys. Chem.* **1995**, *99*, 5269.
(39) Suzuki, K.; Kuchitsu, K. *Bull. Chem. Soc. Jpn.* **1977**, *50*, 1905.
(40) Bell, R. J. *Introductory Fourier Transform Spectroscopy*; Academic Press, **1972**.
(41) Chikan, V.; Fournier, F.; Leone, S. R.; Nizamov, B. *J. Phys. Chem. A* **2006**, *110*, 2850.
(42) Heimann, P. A.; Koike, M.; Hsu, C. W.; Blank, D.; Yang, X. M.; Suits, A. G.; Lee, Y. T.; Evans, M.; Ng, C. Y.; Flaim, C.; Padmore, H. A. *Rev. Sci. Instrum.* **1997**, *68*, 1945.
(43) Griffiths, P. R. *Fourier Transform Infrared Spectrometry*; Wiley: New York, 1986.
(44) Suits, A. G.; Heimann, P.; Yang, X. M.; Evans, M.; Hsu, C. W.; Lu, K. T.; Lee, Y. T.; Kung, A. H. *Rev. Sci. Instrum.* **1995**, *66*, 4841.
(45) Linstrom, P. J., Mallard, W. G., Eds. *NIST Chemistry WebBook*; NIST Standard Reference Database Number 69; National Institute of Standards and Technology: Gaithersburg, MD, June 2005; 20899 (http://webbook.nist.gov).
(46) Lee, L. C. *J. Phys. B: At. Mol. Opt. Phys.* **1977**, *10*, 3033.
(47) Asbrink, L.; Von Niessen, W.; Bieri, G. *J. Electron. Spectrosc. Relat. Phenom.* **1980**, *21*, 93.
(48) Lake, R. F.; Thompson, H. *Proc. R. Soc. London, A* **1970**, *317*, 187.
(49) Gochel-Dupuis, M.; Delwiche, J.; Hubin-Franskin, M.-J.; Collin, J. E. *Chem. Phys. Lett.* **1992**, *193*, 41.
(50) Herzberg, G. *Molecular Spectra and Molecular Structure 1. Spectra of Diatomic Molecules*; Van Nostrand: New York, 1950.

(51) Luque, J.; Crosley, D. R. *LIFBASE: Database and Spectral Simulation Program (Version 1.5*); SRI International Report MP 99-009, 1999.
(52) Luque, J.; Crosley, D. R. *J. Chem. Phys.* **1996**, *104*, 2146.
(53) Levine, R. D.; Bernstein, R. B. *Molecular Reaction Dynamics and Chemical Reactivity*; Oxford University Press: Oxford, U.K., 1987.
(54) Levine, R. D.; Bernstein, R. B. *Acc. Chem. Res.* **1974**, *7*, 393.
(55) Muckerman, J. T. *J. Phys. Chem.* **1989**, *93*, 179.
(56) Sorkhabi, O.; Blunt, V. M.; Lin, H.; Xu, D. D.; Wrobel, J.; Price, R.; Jackson, W. M. *J. Chem. Phys.* **1997**, *107*, 9842.
(57) Nicholls, R. W.; Amani, M.; Mandelman, M. *Can. J. Phys.* **2001**, *79*, 611.
(58) Zachwieja, M. *J. Mol. Spectrosc.* **1995**, *170*, 285.
(59) Danylewych, L. L.; Nicholls, R. W. *Proc. Roy. Soc. London, A* **1978**, *360*, 557.
(60) Hatano, Y. *Phys. Rep.* **1999**, *313*, 109.
(61) Yang, X.; Satoshi, M.; Ohno, K. *J. Phys. Chem. A* **2005**, *109*, 7319.
(62) Jackson, W. M. *J. Chem. Phys.* **1974**, *61*, 4177.
(63) Becker, K. H.; Brenig, H. H.; Tatarczyk, T. *Chem. Phys. Lett.* **1980**, *71*, 242.
(64) Kassner, C.; Stuhl, F. *Chem. Phys. Lett.* **1994**, *222*, 425.
(65) Bobejdijk, M.; van der Zande, W. J.; Kistemaker, P. G. *Chem. Phys.* **1994**, *179*, 125.
(66) Lias, S. G.; Bartmess, J. E.; Liebman, J. F.; Holmes, J. L.; Levin, R. D.; Mallard, W. G. *J. Phys. Chem. Ref. Data* **1988**, *17* (Suppl. 1).
(67) Ma, G.; Suto, M.; Lee, L. C. *J. Quant. Spectrosc. Radiat. Transfer* **1990**, *44*, 379.
(68) Hess, W. P.; Leone, S. R. *J. Chem. Phys.* **1987**, *86*, 3773.
(69) Marinelli, W. J.; Sivakumar, N.; Houston, P. L. *J. Phys. Chem.* **1984**, *88*, 6685.
(70) Nadler, I.; Mahgerefteh, D.; Reisler, H.; Witting, C. *J. Chem. Phys.* **1985**, *82*, 3885.
(71) Poutsma, J. C.; Upshaw, S. D.; Squires, R. R.; Wenthold, P. G. *J Phys. Chem. A* **2002**, *106*, 1067.